

Magnetic force micropiston: An integrated force/microfluidic device for the application of compressive forces in a confined environment

J. K. Fisher and N. Kleckner

Citation: [Review of Scientific Instruments](#) **85**, 023704 (2014); doi: 10.1063/1.4864085

View online: <http://dx.doi.org/10.1063/1.4864085>

View Table of Contents: <http://scitation.aip.org/content/aip/journal/rsi/85/2?ver=pdfcov>

Published by the [AIP Publishing](#)

Articles you may be interested in

[Modeling and validation of autoinducer-mediated bacterial gene expression in microfluidic environments](#)
Biomicrofluidics **8**, 034116 (2014); 10.1063/1.4884519

[Microfluidic devices for cell cultivation and proliferation](#)
Biomicrofluidics **7**, 051502 (2013); 10.1063/1.4826935

[Transport and shear in a microfluidic membrane bilayer device for cell culture](#)
Biomicrofluidics **5**, 022213 (2011); 10.1063/1.3576925

[Release monitoring of single cells on a microfluidic device coupled with fluorescence microscopy and electrochemistry](#)
Biomicrofluidics **4**, 043009 (2010); 10.1063/1.3491470

[A microfluidic device for physical trapping and electrical lysis of bacterial cells](#)
Appl. Phys. Lett. **92**, 214103 (2008); 10.1063/1.2937088

Nor-Cal Products



Manufacturers of High Vacuum
Components Since 1962

- Chambers
- Motion Transfer
- Flanges & Fittings
- Viewports
- Foreline Traps
- Feedthroughs
- Valves



www.n-c.com
800-824-4166

Magnetic force micropiston: An integrated force/microfluidic device for the application of compressive forces in a confined environment

J. K. Fisher^{a)} and N. Kleckner

Department of Molecular and Cellular Biology, Harvard University, Cambridge, Massachusetts 02188, USA

(Received 8 September 2013; accepted 20 January 2014; published online 11 February 2014)

Cellular biology takes place inside confining spaces. For example, bacteria grow in crevices, red blood cells squeeze through capillaries, and chromosomes replicate inside the nucleus. Frequently, the extent of this confinement varies. Bacteria grow longer and divide, red blood cells move through smaller and smaller passages as they travel to capillary beds, and replication doubles the amount of DNA inside the nucleus. This increase in confinement, either due to a decrease in the available space or an increase in the amount of material contained in a constant volume, has the potential to squeeze and stress objects in ways that may lead to changes in morphology, dynamics, and ultimately biological function. Here, we describe a device developed to probe the interplay between confinement and the mechanical properties of cells and cellular structures, and forces that arise due to changes in a structure's state. In this system, the manipulation of a magnetic bead exerts a compressive force upon a target contained in the confining space of a microfluidic channel. This magnetic force microfluidic piston is constructed in such a way that we can measure (a) target compliance and changes in compliance as induced by changes in buffer, extract, or biochemical composition, (b) target expansion force generated by changes in the same parameters, and (c) the effects of compression stress on a target's structure and function. Beyond these issues, our system has general applicability to a variety of questions requiring the combination of mechanical forces, confinement, and optical imaging.

© 2014 AIP Publishing LLC. [<http://dx.doi.org/10.1063/1.4864085>]

I. INTRODUCTION

In the last two decades, investigations into the force response of biological specimen at the cellular to the single molecule length scales have become increasingly common. When manipulating larger objects (typically on the μm length scale), devices that apply both tensile and compressive stresses are used frequently, while investigations at the single molecule level typically only involve the application of tensile stresses. For example, instruments with physical connections to probes such as atomic force microscopes (AFMs) have been used to apply relatively large forces (up to hundreds of μN) with pN sensitivity to cells,^{1–3} components of blood clots,⁴ to multiple bio-molecules at a time,⁵ and to probe populations of receptor-ligand interactions.⁶ Additionally, attached probe techniques using micropipettes or microneedles have been used to determine mechanical properties such as the bending rigidity of mitotic chromosomes,⁷ and to determine the role lamins and chromatin play in maintaining the integrity of the nucleus.^{8,9}

For manipulating smaller objects, detached probe techniques that apply forces via electric fields (laser tweezers) or magnetic fields (magnet based manipulation) are often employed. In these experiments the applied forces typically need not be as large; up to hundreds of pN for laser tweezers and tens of nN for magnetic based manipulation, but much higher force sensitivity (on the order of 0.01 pN) is advantageous. Typical experiments utilizing these systems include investigations of the mechanical properties of sin-

gle molecules of DNA,^{10–13} tensile forces required to disrupt DNA-nucleosome interactions¹⁴ and the higher order packaging of nucleosomes,¹⁵ and investigations of force induced signal transduction in cells.¹⁶

Experimental systems that apply compression forces are less common than those applying tensile forces, and until very recently have remained limited to attached probe techniques such as macroscopic plates,¹⁷ microplates,^{18,19} microindenters,^{20,21} and AFMs.^{1,9,22} In these systems, compression is achieved by pressing the manipulated object into a substrate that acts as a one-dimensional physical barrier. The compressed object is then free to redistribute in the other dimensions, as shown in Fig. 1(a). An alternative manipulation scheme that uses a reduction in confining volume to apply a compressive force, while minimizing the potential for redistribution, is shown in Fig. 1(b).

Most recently and most closely related to the aims of this work, a system using an optical trap to manipulate a bead inside a microfluidic channel for the purposes of combining compressive forces and confinement has been reported.²³ This system is capable of applying forces as large as 100 pN to compress isolated bacterial nucleoids using a high power (up to 4 W) laser to generate forces. Localized heating generated by the trapping/manipulation laser, which could be as high as 40 °C in water for a laser of their wavelength and power and significantly higher in other media,²⁴ may compromise the ability of such a system to apply compressive forces without causing significant damage to the specimen. Our desire to apply compressive forces to biological targets under confinement, in a system closely replicates the target's natural environment, has led to the development of the device described herein.

^{a)} Author to whom correspondence should be addressed. Electronic mail: jfisher@mcb.harvard.edu

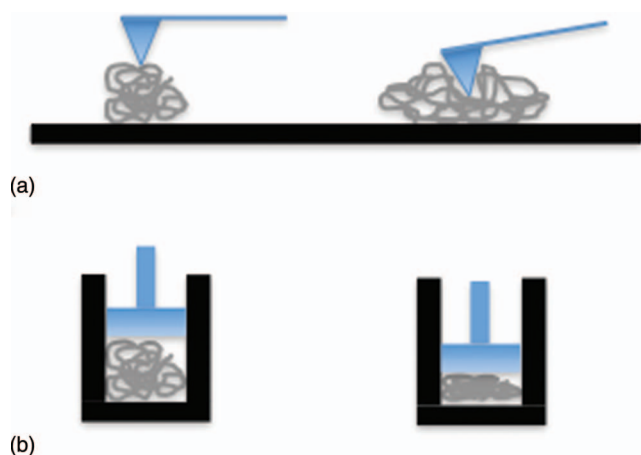


FIG. 1. Compression with and without confinement. In part (a) compressive forces are applied to a molecule in a system without complete confinement, allowing the molecule to reposition itself in response to the force. (b) Compressive force applied in a system that does not permit large scale repositioning of the target.

II. EXPERIMENTAL SETUP

A. Design and fabrication of the magnetic force micropiston

The micropiston system consists of two main components: (1) the microfluidic subsystem responsible for isolating the specimen, providing confinement and buffer exchange, and (2) the magnetic subsystem which is used to manipulate magnetic beads for the purpose of applying compressive forces (pressures) to the specimens.

The microfluidic component of this device is made of two large channels that are interconnected via a series of small channels or compression chambers (Figs. 2(a) and 2(b)). At the output end of each compression chamber a constriction acts to block the passage of larger objects, thus trapping these objects in the chamber while maintaining the ability to exchange buffers and deliver biological targets (e.g., proteins) to the compression chambers.

To fabricate the microfluidic device, we begin with a 4 in. silicon wafer that is coated with a 2 μm thick layer of photoresist (S1813, Shipley Company, Marlborough, MA). A standard photolithographic process is used to pattern the photoresist with the X-Y dimensions of the compression chambers as defined in a photomask. The Z dimension is then defined by etching the resist free regions of the wafer using a reactive ion etch (Surface Technology Systems ICP RIE, located in the Harvard Center for Nanoscale Systems), turning the areas protected by the resist into ridges (Fig. 3(a)). The protective photoresist is then removed, leaving behind finished compression chambers that are 100 μm long, with widths and heights that are just slightly larger than the diameters of commercially available 1.0, 2.8, and 4.5 μm magnetic beads (one wafer per bead diameter). As a result, the compression chambers are 1.05, 2.85, or 4.55 (± 0.05) μm wide and tall, narrowing down to 0.5–2 μm wide in the constricted area (constrictions seen in Fig. 2(b)).

After the compression chambers have been fabricated, two large channels, 100 μm wide and 50 μm tall, perpen-

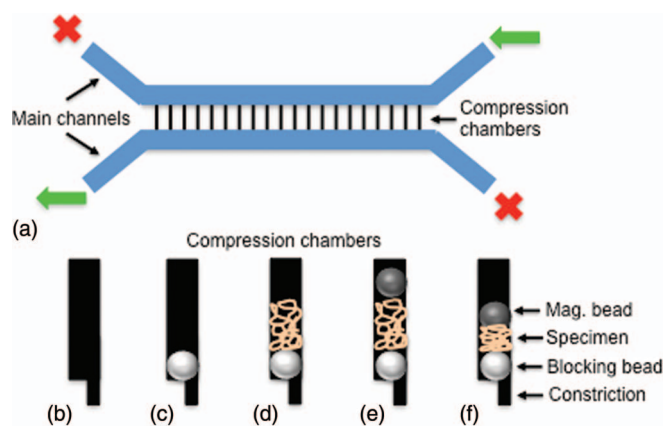


FIG. 2. Cartoon representation of the operation of the micropiston system showing the entire device (a) and zoomed-in view of the microchannels [(b)–(f)]. In part (a), valves at the upper right and lower left of the device are open, allowing fluid to flow from the upper main channel, across the small channels (compression chambers) with constrictions and into the second large channel. The direction of fluid flow is indicated with green arrows, closed valves preventing fluid flow are indicated with a red X. Parts (b)–(f) depict loading the device. Empty compression chambers (b) are first loaded with polystyrene blocking beads that prevent passage of the compression target (c). (d) Using fluid flow, compression targets (tan line) are loaded into the chambers. (e) Magnetic beads are then loaded into the chambers using weak fluid flow. After magnetic bead loading, all valves are closed and the system is allowed to equilibrate prior to the application of force. (f) Compressive forces are applied by actuating the magnetic beads in the direction of the polystyrene blocking beads (down the channel).

dicular to the ends of the small channel are made from SU-8 2050 (Microchem, Newton, MA) (Fig. 3(b)) via photolithography. These channels are responsible for delivering fluid to the input side of compression chambers and collecting fluid that has passed through to the output side. The resulting two-layer mold is then treated with trichlorosilane (Gelest Inc., Morrisville, PA) to reduce adhesion between the wafer and the mold material.

To generate forces inside the small microfluidic channels, 100 μm thick magnetic foils (Netic® alloy, Magnetic Shield Corporation, Bensenville, IL) couple the magnetic fields generated by a six-core electromagnet system (discussed in detail below) to the microfluidic channels described above. The magnetic foils are etched (Fotofab, Chicago, IL) to create a rectangular frame that surrounds a total of 6 arms (one arm for each of the six electromagnets). Three of these arms (top 3 in Figs. 3(c) and 3(d)), which are coupled to three of the electromagnets and driven with a like polarity current, merge into a rectangular block. The other three arms (bottom 3 in Figs. 3(c) and 3(d), seen in detail in Fig. 3(e)) are coupled to the remaining three electromagnets and driven with the opposite polarity and terminate as sharp tips. The sharp tips generate the high field gradients necessary to achieve large magnetic forces. The rectangular block, located 500 μm away from the tips, serves as a return path for the magnetic flux back into the drive ring of the six-core electromagnet system. This geometry provides a low resistance (reluctance) loop that will maximize the magnetic field at a given magnetomotive force according to the following equation:

$$\text{mmf} = \Phi R,$$

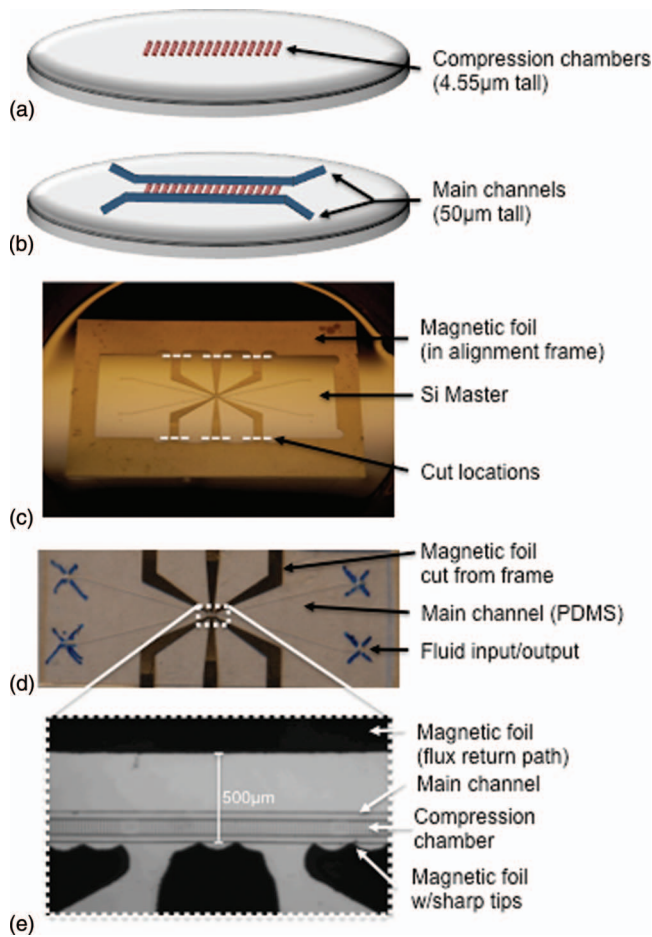


FIG. 3. Device construction. (a) Small channels (“compression chambers”) are created first by etching away the surrounding silicon wafer. (b) Two large “main” channels made from SU-8 are added to the wafer, completing the silicon master. (c) Etched thin magnetic foils are placed atop the Si master, covered in PDMS, and cured for 2 h at 65 °C. The foils are cut along the dashed white lines to separate the micropiston chip from the alignment frame. (d) Completed micropiston chip peeled away from the Si wafer and cut from the alignment frame. Holes punched in the backside of the PDMS (indicated with blue “X”) are used to deliver fluid to the microfluidic channels. (e) Zoomed-in view of the microfluidic channels and the etched magnetic materials.

where mmf is the magneto-motive force, Φ is the magnetic flux, and R the reluctance. The large rectangular frame (Fig. 3(c)) preserves the alignment of the tips and the rectangular block until they become incorporated into the final device.

Micropiston “chips” are made by incorporating the magnetic foils into a polydimethylsiloxane (PDMS) (Slygard 184, Dow Corning, Midland, MI) based microfluidic mold of the silicon wafer (master). This is accomplished by mounting the etched magnetic foil on the silicon master with the tips aligned 1–10 μm from the large channel closest to the constrictions. PDMS is then poured over the master and magnetic foil, degassed, and cured at 65 °C for 2 h. Once cured, the PDMS with embedded magnetic foil is peeled away from the silicon master and holes are punched in the PDMS at the fluid input/output locations (blue “X”s in Fig. 3(d)). The elevated features of silicon master are now trenches in the PDMS mold that, once sealed, can be used to hold and deliver fluid. The

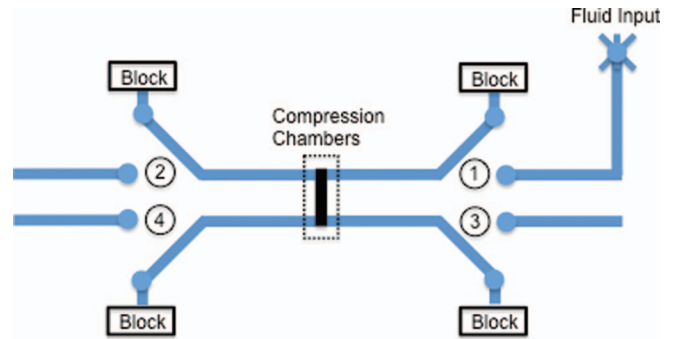


FIG. 4. Fluidic circuit. The micropiston “chip” containing the compression chambers is connected to an external fluid delivery system using four valves (numbered 1–4) that either deliver fluid to the input/output side of a main channel or isolate the chip from the fluid delivery system.

process of embedding the magnetic foil in the PDMS typically results in a 1–5 μm layer of cured PDMS between the top of the silicon master and the surface of the magnetic foil that was in close contact with the silicon master. The presence of this thin layer means that there is a continuous layer of PDMS on the “bottom” of the device that may be bonded to a piece of glass to seal the back side of the channels. To create this seal, the PDMS is activated via oxygen plasma and bonded to a 24 \times 60 mm coverslip. The micropiston chip is completed by cutting the magnetic foil’s large rectangular frame at the base of the arms (cut locations indicated with white dashed lines in Fig. 3(c)), leaving isolated magnetic structures that will be energized by individual electromagnets (Fig. 3(d)). A high magnification view of the magnetic foils, main channels, and compression channels is shown in Fig. 3(e).

Fluid is delivered to/removed from the micropiston chip via two acrylic manifolds, each with two ports that couple teflon tubing (#1527L, IDEX Health & Science, Oak Harbor, WA) from the off-chip fluid delivery/removal system to the chip via 0.5 mm passages in the manifold. Fluid input to the off-chip delivery/removal system is selected using a 6-port selection valve (V-240, IDEX Health & Science) that is used in conjunction with a syringe pump (Model 100, KD Scientific Inc., Holliston, MA) for precise flow rate control. Prior to entering the chip, the fluid passes through a 4-way right angle flow valve (V-100L, IDEX Health & Science) (valve 1 in Fig. 4) that, along with the three other 4-way valves at each of the chip’s input/outputs (valves 2–4 in Fig. 4), are used to control fluid flow through the chip. To load the chip, valves 1 and 4 are opened (valves 2 and 3 closed), allowing fluid to flow from the top main channel, down the compression chambers, through the constrictions, and into the bottom main channel. Once the chip is loaded, all valves are closed (switched to “block” in Fig. 4) to isolate the chip and prevent unwanted fluid flow.

The magnetomotive force used to actuate magnetic beads in compression chambers is provided by the six independently controlled electromagnets previously described as part of a thin-foil magnetic force system for high-numerical-aperture microscopy.²⁵ Briefly, this system consists of a castellated annular magnetic drive ring with each of the six evenly spaced castellations wound with magnet wire. Magnetomotive force

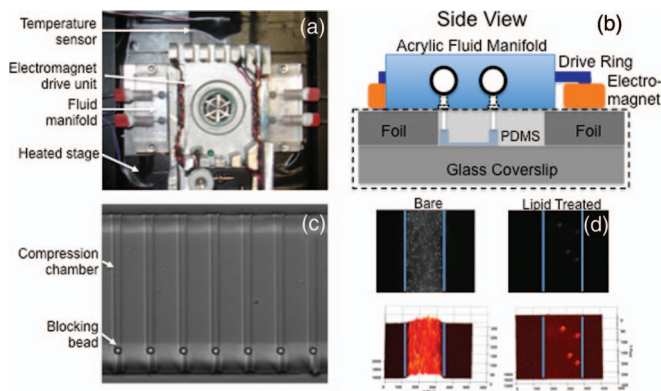


FIG. 5. (a) The complete micropiston system, with the electromagnet drive unit in the center flanked by acrylic fluid delivery manifolds. These three components sit atop a heated plate (surface covered with black insulation) inserted into the 96-well plate adapter of a motorized stage (Proscan II, Prior Scientific, Rockland, MA). (b) Illustrated side view of the micropiston chip (dashed black rectangle), fluid manifold, and electromagnets. (c) Multiple compression chambers (small channels) of the micropiston system loaded with $4.5\ \mu\text{m}$ blocking beads. (d) Non-specific adsorption to the inner channel surfaces is reduced significantly using a lipid treatment. The top two images are unprocessed fluorescence, bottom two have fluorescent intensity mapped to surface height. Blue lines indicate channel walls. The adsorption of 200 nm polystyrene beads to channel surfaces after a 2 h incubation is shown for a bare channel (left) and treated channel (right).

is controlled by sending a voltage from a digital to analog converter (DAC) board (National Instruments, PCI-6713, Woburn, MA) to a six-channel transconductance drive amplifier with a gain of 0.5 A/V. This current is sent to the electromagnets where it produces a magnetic field that is coupled into the magnetic foil embedded in the chip.

The micropiston chip and electromagnets, as well as an acrylic manifold used to deliver fluid to the chip, sit atop a $3/16$ in. thick heated aluminum plate coated with black insulating tape (all seen in Figure 5(a)), designed to fit in the 96-well plate adaptor commonly available for translation stages on commercial microscopes. The temperature of the plate is maintained by a closed loop temperature controller (Oven Industries, Model 5C7-195, Mechanicsburg, PA) connected to two cartridge heaters (Omega, Stamford, CT, CSS-01235) inserted into holes drilled into the side of the $3/16$ in. plate, with the temperature monitored by either a thermocouple (Omega, CHAL-001-36) inserted into the microfluidic chip or a sensor mounted on the aluminum plate (Oven Industries, TS104). A cartoon illustration of a cross-sectional side view of the system is seen in Fig. 5(b). The micropiston chip consists of all of the components contained inside the dashed rectangle. Note the thin layer of PDMS (light grey) between the foil and coverslip that is used to bond the coverslip to the rest of the chip. The fluid manifolds and electromagnets couple directly to the top of this chip, with the screws that hold the fluid manifolds to the aluminum plate responsible for securing the chip against the plate as well. An example of a micropiston chip loaded with non-magnetic blocking beads is seen in Fig. 5(c). All chambers typically load with a single blocking bead initially instead of multiple beads entering a few chambers due to the decrease in intrachamber fluid flow that comes with partial blockage.

In order to prevent non-specific adsorption of injected materials onto the channel walls, shortly after sealing the device a buffer solution containing 1 mg/ml concentration of small lamellar vesicles (SUVs), in this case egg phosphatidylcholine, (Avanti Polar Lipids, Alabaster, AL) is injected into the channels as described by Yang *et al.*,²⁶ causing the spontaneous formation of a lipid bilayer on the inner surfaces of the channels via vesicle fusion.²⁷ The effectiveness of this technique was verified by checking for non-specific adsorption of fluorescently labeled 200 nm polystyrene beads after prolonged exposure to the channel surfaces. Both lipid treated and non-treated devices were loaded with the beads, allowed to incubate for 2 h, and then washed with phosphate buffered saline (PBS). As seen in Figure 5(d), non-specific adsorption of the beads was greatly reduced for the channels treated with the lipids (channel walls indicated with blue lines). As a result of this effectiveness, all results presented here are for channels that have been treated with the lipids prior to introduction of a specimen.

III. RESULTS

A. Blocking beads: Effectiveness of blocking channel outputs

As seen in the conceptual cartoon of our system, in order to facilitate rapid (not diffusion driven) buffer exchange we use a non-magnetic “blocking” bead atop a constriction at the base of the compression channel to allow fluid to flow through the channel while restricting passage of larger target objects. To test the functionality of this technique, we injected $4.5\ \mu\text{m}$ polystyrene beads into the system to block the exit of the compression channels. With the polystyrene beads in place, the available area for passage through the channel is reduced from one region with an area of $20.70\ \mu\text{m}^2$ ($4.55 \times 4.55\ \mu\text{m}$) to two passages each with an area $1.21\ \mu\text{m}^2$.

With the polystyrene blocking beads in place, we then flowed fluorescently labeled (Sytox Green, S7020, Invitrogen, Grand Island, NY) linearized lambda DNA (New England Biolabs, N3011S, Ipswich, MA) molecules into the system at a rate of $0.5\ \mu\text{L/h}$. As seen in Fig. 6, the majority of the lambda DNA molecules are unable to fit past the blocking bead(s) and collect in the compression chamber.

B. Buffer exchange: Decondensation of xenopus sperm chromatin driven by media exchange

To test the ability of our device to bring forth a change in the state of a biological target via buffer exchange, we used a *Xenopus laevis* system to generate interphase-like chromatin from demembrated sperm heads. Sperm heads suspended in “Buffer X” (10 mM HEPES, 80 mM KCl, 15 mM NaCl, 5 mM MgCl_2 , 1 mM EDTA) are loaded in the channels of the micropiston between a blocking bead and a magnetic bead. The sperm specific buffer is then replaced with egg extract diluted with “EB” buffer (250 mM sucrose, 75 mM KCl, 0.5 mM spermidine trihydrochloride, 0.2 mM spermine tetrahydrochloride, pH 7.3–7.5) before closing the input/output valves of the microfluidic subsystem. Incubation

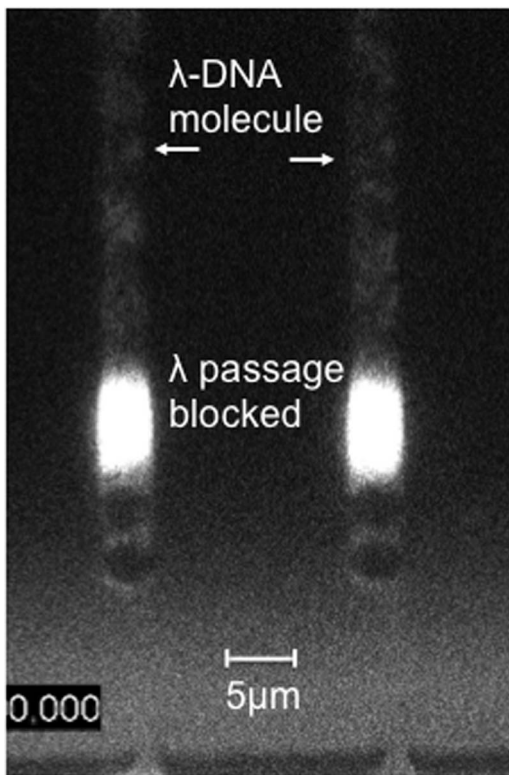


FIG. 6. Blocking beads in microfluidic channels capturing lambda DNA. The passage of fluorescently labeled lambda DNA through the microfluidic channels is significantly hindered by the introduction of $4.5 \mu\text{m}$ blocking beads.

of the demembrated sperm head in the extract causes the chromatin to expand, exerting pressure on the beads which in turn forces the magnetic bead up the channel (away from the blocking bead). The rate of this expansion is dependent upon the dilution factor of the extract, with expansion typically taking approximately 1 h for an extract diluted $3\times$ in extract buffer.

As seen in Fig. 7, expansion of the sperm chromatin due to exposure to the egg extract is a dramatic effect that causes the magnetic beads to be pushed over distances of many μm . Interestingly, the pressures associated with this type of expansion are much greater than the maximum pressure that our device can apply in opposition, requiring the use of fluid forces to push on the upper magnetic bead to compress the chromatin.

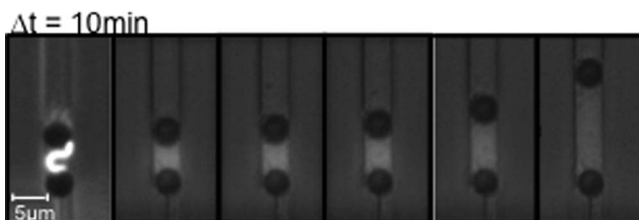


FIG. 7. Bead movement driven by chromatin expansion. Exposure of the sperm chromatin (bright material between dark beads) to egg extract causes the chromatin to decompact, pushing the bead towards the top of the channel. Here, chromatin expansion pushes the magnetic bead over $10 \mu\text{m}$ in the compression chamber.

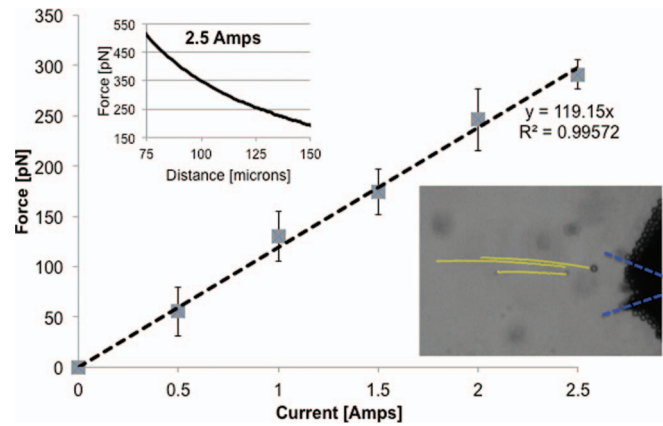


FIG. 8. Magnetic force as a function of drive current. (Upper left) Magnetic force as a function of distance to the pole tip for a 2.5 A current. (Lower right) Example trajectories for $4.5 \mu\text{m}$ beads using in these experiments.

C. Compression forces: Force on a $4.5 \mu\text{m}$ bead

Forces generated by the magnetic system have been calibrated outside of the piston system, as a function of the drive current, by determining the velocity of $4.5 \mu\text{m}$ superparamagnetic beads (Dynabeads M-450, Invitrogen Dynal AS, Oslo, Norway) in solution of known viscosity (Glycerol @ 30°C). With the viscosity (η), bead radius (a_p), and the bead velocity (v) known, we can use Stokes formula, $F = 6\pi\eta a_p v$, to calculate the applied force. Here, $\eta = 5.98 \text{ P}$,²⁸ and $a_p = 2.25 \mu\text{m}$. Using the one-dimensional velocity corresponding to motion down the microchannel in the appropriate Z -plane, the relevant force for a micropiston system may be determined. Here, we restrict our calibration to those beads that are captured by a 30° angle from the pole tip (blue dashed lines in inset image in Fig. 8), corresponding to beads with the majority of the force down the channel. Maximum values of approximately 300 pN are generated in the system's current configuration (average force for a $4.5 \mu\text{m}$ bead 115–125 μm from the pole tip), corresponding to the maximum force applied in a typical micropiston experiment. As seen in the inset figure, force increases dramatically as the distance between the bead and the pole tip decreases. By reducing the width of the main channels, thus decreasing the separation between the bead and the pole, the maximum applied force could be increased significantly, up to 500 pN for a $50 \mu\text{m}$ wide main channel. For applications requiring higher forces, multiple magnetic beads may be used in a single compression channel at one time (see Figure 9(b)).

D. Piston at work

Actuation of the completed micropiston device is shown in Fig. 9. In part A, magnetic forces are used to drive a $4.5 \mu\text{m}$ superparamagnetic bead towards the constricted end of the channel and sub-pN fluid forces are used to return the bead to its original position. In a typical experiment magnetic forces are only used to move the bead towards the constriction, with the bead returning towards its initial position when the compressed material relaxes in the absence of an applied force (electromagnets turned off). In Fig. 9(b), two separate

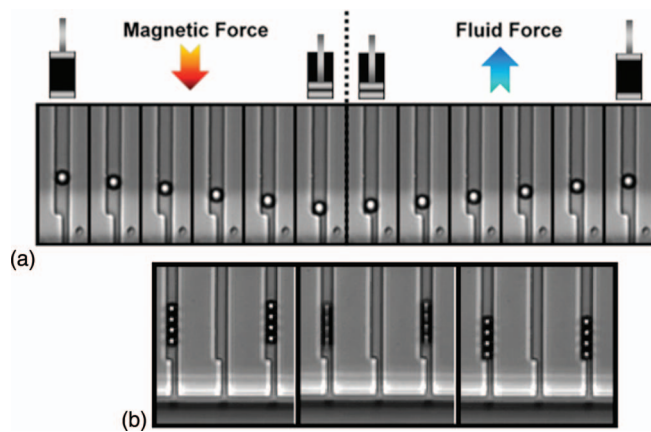


FIG. 9. Piston in action. (a) Montage showing individual frames of a compression cycle in the micropiston. Force towards the constricted end of the channel is generated by the magnetic force sub-system, return force generated by fluid flow. (b) Two compression chambers, each loaded with four magnetic beads, are actuated producing approximately 1.2 nN in each chamber.

compression chambers, each with four beads, are actuated simultaneously with a 2.5 A drive signal. The number of beads used serves as a force multiplier, in this case generating compressive force in these two chambers of 1.2 nN (4 beads \times 300 pN/bead).

IV. SUMMARY

We describe a combination microfluidic, magnetic force system for the application of compressive forces to biological targets under confinement that is compatible with widely available commercial microscope components, including high numerical aperture (N.A.) objectives. This magnetic force micropiston is capable of applying compressive forces in excess of 300 pN on a single bead, and greater than 1 nN (approximately $10\times$ greater than any similar system) when used with multiple magnetic beads in a single compression chamber. The use of magnetic forces eliminates concerns of potentially damaging localized heating associated with laser based manipulation systems. Additionally, the use of magnetic forces allows multiple compression chambers to be operated in parallel, making high throughput experiments a future possibility. Applications of this instrument include measurements of biopolymer stiffness and expansion forces generated by polymers and cells, all as a function of buffer or extract composition, as well as the determination of the effects of compressive stresses on biological polymers and cells. More specifically, we plan to use this instrument to study the role of confinement in generating the previously observed helical structure of the *E. coli* nucleoid.²⁹

ACKNOWLEDGMENTS

This work was supported by the National Institutes of Health Grant No. NIH/NIGMS-R01-GM025326. We acknowledge the Center for Computer Integrated Systems for Microscopy and Manipulation at UNC Chapel Hill, funded by

NIH grant NIBEB-5-P41-EB002025 for providing equipment and analysis tools, and the Center for Nanoscale Systems (CNS) at Harvard University, a member of the National Nanotechnology Infrastructure Network. Additionally, we would like to thank the N. Francis lab for the use of the materials required for the *Xenopus* chromatin experiments.

- ¹V. Lulevich, T. Zink, H. Y. Chen, F. T. Liu, and G. Y. Liu, *Langmuir* **22**(19), 8151–8155 (2006).
- ²P. A. Janmey and C. A. McCulloch, *Annu. Rev. Biomed. Eng.* **9**, 1–34 (2007).
- ³V. Swaminathan, K. Myhre, E. T. O'Brien, A. Berchuck, G. C. Blobel, and R. Superfine, *Cancer Res.* **71**(15), 5075–5080 (2011).
- ⁴M. Guthold, W. Liu, B. Stephens, S. T. Lord, R. R. Hantgan, D. A. Erie, R. M. Taylor, Jr., and R. Superfine, "Visualization and mechanical manipulations of individual fibrin fibers suggest that fiber cross section has fractal dimension 1.3," *Biophys. J.* **87**(6), 4226–4236 (2004).
- ⁵M. Rief, M. Gautel, F. Oesterhelt, J. M. Fernandez, and H. E. Gaub, *Science* **276**(5315), 1109–1112 (1997).
- ⁶H. Y. Yang, J. P. Yu, G. Fu, X. L. Shi, L. Xiao, Y. Z. Chen, X. H. Fang, and C. He, *Exp. Cell Res.* **313**(16), 3497–3504 (2007).
- ⁷M. G. Poirier, S. Eroglu, and J. F. Marko, *Mol. Biol. Cell.* **13**(6), 2170–2179 (2002).
- ⁸J. D. Pajeroski, K. N. Dahl, F. L. Zhong, P. J. Sammak, and D. E. Discher, *Proc. Natl. Acad. Sci. U.S.A.* **104**(40), 15619–15624 (2007).
- ⁹A. Mazumder, T. Roopa, A. Basu, L. Mahadevan, and G. V. Shivashankar, *Biophys. J.* **95**(6), 3028–3035 (2008).
- ¹⁰C. Bustamante, J. F. Marko, E. D. Siggia, and S. Smith, *Science* **265**(5178), 1599–1600 (1994).
- ¹¹K. Hatch, C. Danilowicz, V. Coljee, and M. Prentiss, *Phys. Rev. E* **75**(5), 051908 (2007).
- ¹²C. Danilowicz, C. Limouse, K. Hatch, A. Conover, V. W. Coljee, N. Kleckner, and M. Prentiss, *Proc. Natl. Acad. Sci. U.S.A.* **106**(32), 13196–13201 (2009).
- ¹³M. D. Wang, H. Yin, R. Landick, J. Gelles, and S. M. Block, *Biophys. J.* **70**(2), 1335–1346 (1996).
- ¹⁴B. D. Brower-Toland, C. L. Smith, R. C. Yeh, J. T. Lis, C. L. Peterson, and M. D. Wang, *Proc. Natl. Acad. Sci. U.S.A.* **99**(4), 1960–1965 (2002).
- ¹⁵M. Kruijthof, F. T. Chien, A. Routh, C. Logie, D. Rhodes, and J. van Noort, *Nature Struct. Mol. Biol.* **16**(5), 534–540 (2009).
- ¹⁶R. J. Mannix, S. Kumar, F. Cassiola, M. Montoya-Zavala, E. Feinstein, M. Prentiss, and D. E. Ingber, *Nat. Nanotechnol.* **3**(1), 36–40 (2008).
- ¹⁷F. Guilak, *J. Biomech.* **28**(12), 1529 (1995).
- ¹⁸O. Thoumine, A. Ott, O. Cardoso, and J. J. Meister, *J. Biochem. Biophys. Methods* **39**(1–2), 47–62 (1999).
- ¹⁹N. Caille, O. Thoumine, Y. Tardy, and J. J. Meister, *J. Biomech.* **35**(2), 177–187 (2002).
- ²⁰E. A. G. Peeters, C. V. C. Bouten, C. W. J. Oomens, and F. P. T. Baaijens, *Med. Biol. Eng. Comput.* **41**(4), 498–503 (2003).
- ²¹J. L. V. Broers, E. A. G. Peeters, H. J. H. Kuijpers, J. Endert, C. V. C. Bouten, C. W. J. Oomens, F. P. T. Baaijens, and F. C. S. Ramaekers, *Human Mol. Gen.* **13**(21), 2567–2580 (2004).
- ²²A. Hategan, R. Law, S. Kahn, and D. E. Discher, *Biophys. J.* **85**(4), 2746–2759 (2003).
- ²³J. Pelletier, K. Halvorsen, B. Y. Ha, R. Paparcone, S. J. Sandler, C. L. Woldringh, W. P. Wong, and S. Jun, *Proc. Natl. Acad. Sci. U.S.A.* **109**(40), E2649–E2656 (2012).
- ²⁴E. J. G. Peterman, F. Gittes, and C. F. Schmidt, *Biophys. J.* **84**(2), 1308–1316 (2003).
- ²⁵J. K. Fisher, J. Cribb, K. V. Desai, L. Vicci, B. Wilde, K. Keller, R. M. Taylor, J. Haase, K. Bloom, E. T. O'Brien, and R. Superfine, *Rev. Sci. Instrum.* **77**(2), 023702 (2006).
- ²⁶T. L. Yang, S. Y. Jung, H. B. Mao, and P. S. Cremer, *Anal. Chem.* **73**(2), 165–169 (2001).
- ²⁷A. A. Brian and H. M. McConnell, *Proc. Natl. Acad. Sci. U.S.A.* **81**(19), 6159–6163 (1984).
- ²⁸N. S. Cheng, *Ind. Eng. Chem. Res.* **47**(9), 3285–3288 (2008).
- ²⁹J. K. Fisher, A. Bourmiquel, G. Witz, B. Weiner, M. Prentiss, and N. Kleckner, *Cell* **153**(4), 882–895 (2013).